High-quality reconstruction of an optical image by an efficient Laguerre-Gaussian mode decomposition method

JIANTAO MA,[1,4] DAN WEI,[1,4] LUYI WANG,[1] YONG ZHANG,[1,2,*] (iD) AND MIN XIAO[1,2,3] (iD)

[1]*National Laboratory of Solid State Microstructures, College of Engineering and Applied Sciences, and School of Physics, Nanjing University, Nanjing 210093, China*
[2]*Collaborative Innovation Center of Advanced Microstructures, Nanjing University, Nanjing 210093, China*
[3]*Department of Physics, University of Arkansas, Fayetteville, AR 72701, USA*
[4]*These authors contribute equally to this work*
[*]*zhangyong@nju.edu.cn*

Abstract: We propose and experimentally demonstrate an optical image reconstruction in the Laguerre-Gaussian (LG) domain. Because LG mode features circular symmetry, it has unique advantages to decompose an image with rotational symmetry. In the experiment, we realize a high-fidelity reconstruction of an optical image by using about 10^4 LG modes. In the proposed configuration, the radial sampling points are much fewer than those in the existing methods, which can significantly improve the efficiency. Furthermore, we show azimuthal image noise reduction through LG domain filtering. Our results open a door for LG-mode based optical image processing.

1. Introduction

Orbital angular momentum (OAM) carrying beams have promoted many fascinating techniques from optical trapping and optical tweezer [1,2] to optical communications [3,4], super-resolution imaging [5], precision measurement [6,7], and quantum information processing [8,9]. Driven by the mapping between azimuthal angle and OAM [10], the recent advances of digital spiral imaging techniques [11–13] have demonstrated that OAM is a promising tool to detect object's geometrical information, such as object's azimuthal identification [14–16], rotating object's sensing [17] and optical image rotation [18]. However, OAM itself is unable to reconstruct a complete optical image.

As a complete and orthogonal basis, Laguerre-Gaussian (LG) mode is a potential candidate to accomplish this task. LG mode [19] carries OAM, which is characterized by an azimuthal index l and a radial index p. LG modes are the Eigen solutions of the paraxial wave equation, which can be used for mode decomposition and optical image processing under paraxial approximation [20]. Particularly, featuring circular symmetry, LG basis has advantages in analyzing the images with rotational symmetry. For example, consider an optical image featuring N-fold circular symmetry. The energy of its LG spectrum is concentrated in the components with their l indices being multiples of N [10,14,17]. In previous researches, many approaches have been proposed to measure OAM spectrum (i.e., l spectrum) [21–27]. However, it still lacks an efficient way to measure the complete LG spectrum (i.e., both l and p spectra) [28,29].

In this letter, we propose a systematic approach to decompose a full optical image based on LG modes. In our method, we calculate the radial mode distribution by adopting least squares fitting. The required radial sampling points are much fewer than those in the existing methods [28,29], which can significantly improve the efficiency. An optimal beam waist is critical to minimize the LG mode number needed for image reconstruction. Furthermore, we demonstrate LG domain

filtering to reduce the azimuthal noise, which shows the potential application in optical image processing.

2. Method

An arbitrary optical image U can be expressed as a coherent superposition of LG modes,

$$U(r, \theta, z) = \sum_{l,p} A_{l,p} LG_{l,p}(r, \theta, z) \tag{1}$$

where $A_{l,p}$ is a complex variable that defines the amplitude and relative phase of LG mode, r is the radius, θ is the azimuthal angle, and z is the propagation distance.

To simplify the analysis, we consider the image expansion at the position of the beam waist ($z=0$). The field distributions of LG modes are given by [20]

$$
\begin{aligned}
LG_{l,p}(r, \theta) = \sqrt{\frac{2p!}{\pi(p+|l|)!}} \frac{1}{w_0} \\
\cdot \left[\frac{r\sqrt{2}}{w_0} \right]^{|l|} \exp\left[\frac{-r^2}{w_0^2} \right] L_p^{|l|}\left(\frac{2r^2}{w_0^2} \right) \exp(il\theta)
\end{aligned}
\tag{2}
$$

where w_0 is the beam waist, and l and p are the azimuthal and radial indices, respectively. $L_p^{|l|}$ is the generalized Laguerre polynomial. According to Eqs. (1) and (2), to expand or reconstruct an optical image U in the LG domain, one should decide the coefficient, the beam waist w_0 and the mode expansion range. Note that all LG modes used for image decomposition are defined by the same w_0.

The LG mode range for image reconstruction is related to l, p, and w_0. As shown in Eq. (2), the azimuthal distribution of the LG mode is related to the helical phase as well as the l index. The azimuthal expansion of an image can be written as

$$
\begin{aligned}
B_l(r) &= \int_0^{2\pi} U(r, \theta)\exp(-il\theta)d\theta \\
&= \sum_p A_{l,p} LG_{l,p}(r)
\end{aligned}
\tag{3}
$$

with $LG_{l,p}(r) = \sqrt{\frac{2p!}{\pi(p+|l|)!}} \frac{1}{w_0} \left[\frac{r\sqrt{2}}{w_0} \right]^{|l|} \exp\left[\frac{-r^2}{w_0^2} \right] L_p^{|l|}\left(\frac{2r^2}{w_0^2} \right)$. $B_l(r)$ shows the radial distribution in different OAM subspaces, which can be understood as the l spectrum at different radius.

Numerical computation of the integral in Eq. (3) is generally time-consuming. Here, we exploit the Fourier relationship between angular position and OAM [10] and calculate Eq. (3) by FFT at each radius after transforming the image U to polar coordinate. In our experiment (Fig. 1(a)), the original image is recorded by a 512×512 CCD detector with 50 μm pixel size and the largest circumference contains 1609 pixels. We set the radial and azimuthal pixels of the target image to be 256 and 1609, respectively (Fig. 1(b)). Here, we adopt the bicubic interpolation to replenish the azimuthal pixel numbers at small radii to 1609.

To ensure high fidelity, we define the truncation l order by using the following criterion,

$$\sum_{l=-m}^{m} P_l(r) = F \cdot P(r) \tag{4}$$

$P(r)$ and $P_l(r)$ are the total power and the power of the l-order component at radius r, respectively. F is a coefficient, which is set as 0.99 in our experiment. Equation (4) indicates that the azimuthal expansion is truncated when the l spectrum from $-m$ order to m order contains 99% power at the corresponding radius. The calculated truncation l order for each radial position is shown
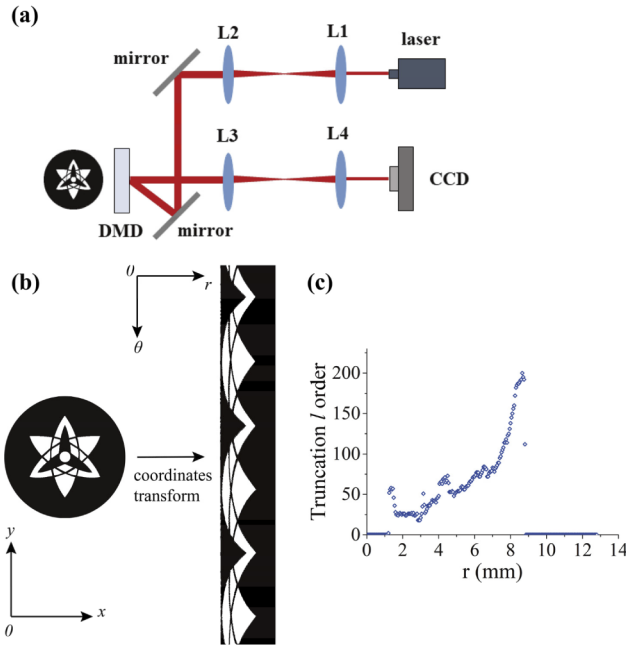
Fig. 1. (a) Experiment setup. The incident beam is from a 1064 nm laser. The image is produced by a DMD (ViALUX, DLP7000) and then recorded by a CCD with 512*512 pixels (Xenics, Lynx-11279). Note that our method works for both coherent and incoherent light illumination. (b) Image transformation from Cartesian coordinates to polar coordinates. (c) The azimuthal truncation l order at each radius.

in Fig. 1(c). The highest order is 200 at $r = 8.65$ mm. It should be noted that, to analyze the p components in $B_l(r)$, the range of the l spectrum at each radius is required to be consistent. Thus, we extract the l components between ± 200 orders to perform the azimuthal expansion. The actual azimuthal expansion accuracy of the whole image is more than 99% in the experiment.

For an arbitrary l order, $B_l(r)$ can be seen as a coherent combination of many p components. Generally, an integral method can be used to calculate the weights of the p components [28,29], in which a large sampling number is required to ensure high accuracy. Here, we propose a method to acquire the mode coefficient with a significantly reduced sampling number.

In experiment, we measure $B_l(r)$ at different radial positions. Then, we can re-write Eq. (3) as a multivariate linear equation with different r,

$$
\begin{bmatrix}
B_l(r_1) \\
B_l(r_2) \\
\vdots \\
B_l(r_m)
\end{bmatrix}
=
\begin{bmatrix}
LG_{l,0}(r_1) & LG_{l,1}(r_1) & \cdots & LG_{l,p}(r_1) \\
LG_{l,0}(r_2) & LG_{l,1}(r_2) & \cdots & LG_{l,p}(r_2) \\
\vdots & \vdots & \cdots & \vdots \\
LG_{l,0}(r_m) & LG_{l,1}(r_m) & \cdots & LG_{l,p}(r_m)
\end{bmatrix}
\cdot
\begin{bmatrix}
A_{l,0} \\
A_{l,1} \\
\vdots \\
A_{l,p}
\end{bmatrix}
\tag{5}
$$

where $r_1, r_2 \ldots r_m$ are different radial position and m is the radial sampling number. There are $p+1$ unknown variables $(A_{l,0}, A_{l,1}, \ldots, A_{l,p})$ to be ascertained.

Equation (5) can be re-written as

$$
B = LG \cdot A
\tag{6}
$$

$$\text{where } B = \begin{bmatrix} B_l(r_1) \\ B_l(r_2) \\ \vdots \\ B_l(r_m) \end{bmatrix}, A = \begin{bmatrix} A_{l,0} \\ A_{l,1} \\ \vdots \\ A_{l,p} \end{bmatrix}, LG = \begin{bmatrix} LG_{l,0}(r_1) & LG_{l,1}(r_1) & \cdots & LG_{l,p}(r_1) \\ LG_{l,0}(r_2) & LG_{l,1}(r_2) & \cdots & LG_{l,p}(r_2) \\ \vdots & \vdots & \cdots & \vdots \\ LG_{l,0}(r_m) & LG_{l,1}(r_m) & \cdots & LG_{l,p}(r_m) \end{bmatrix}.$$

In our method, the minimal radial sampling number is $p+1$ to decide the radial mode coefficient; this is much smaller than that in integral method [28,29]. When the radial sampling number m is larger than $p+1$, Eq. (6) forms an over-determined system of equations, which is solved by calculating its least-square solution,

$$A^* = arg \min_x ||LG \cdot A - B||^2 = (A^T A)^{-1} A^T b \tag{7}$$

where $(A^T A)^{-1} A^T$ is the pseudo-inverse matric of A. The least-square fitting is implemented by QR decomposition algorithm.

To demonstrate the advantage of this fitting method, we analyze several LG mode fields ($p=8$ in Fig. 2(a), $p=50$ in Fig. 2(b), and $p=9, 15, 28$ superposed with 1:2:1 amplitude ratio in Fig. 2(c)).
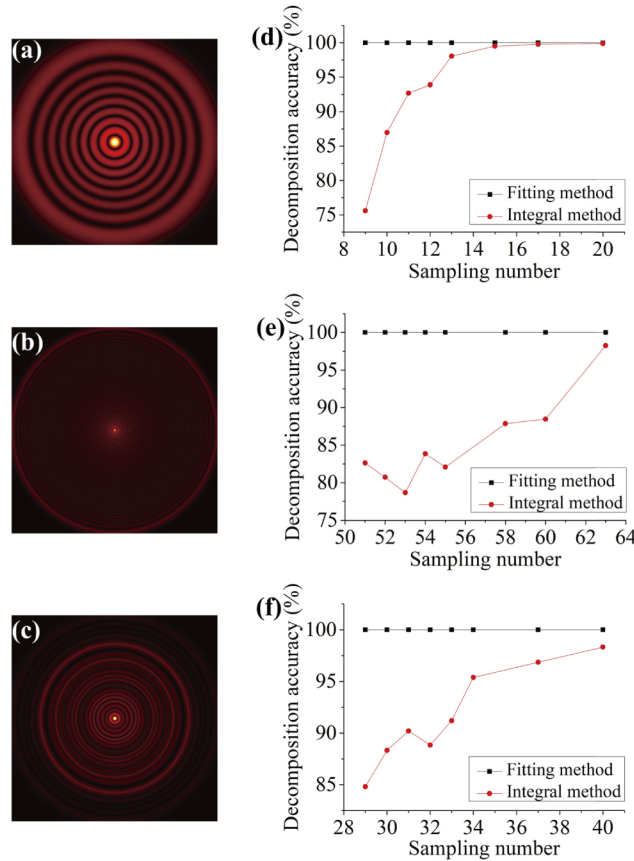

Fig. 2. Comparison of least squares fitting and the integral method. The target images are (a) a pure LG mode with $p=8$ and $w_0=3000\,\mu m$, (b) a pure LG mode with $p=50$ and $w_0=1260\,\mu m$, and (c) a superposed LG field with $p=9, 15, 28$ (1:2:1 amplitude ratio) and $w_0=1700\mu m$. The decomposition accuracy in (d)-(f) corresponds to the fields in (a)-(c), respectively.

Note that LG modes with $l=0$ are used since we focus on the radial components here. The decomposition accuracy is defined by

$$\eta = 1 - \frac{\sum_p |A_p^s - A_p^0|^2}{\sum_p |A_p^0|^2} \tag{8}$$

where A_p^0 and A_p^s are the theoretical and calculated coefficients of the LG modes, respectively. As shown in Figs. 2(d)–2(f), in comparison to the integral method, the least squares fitting method can well preserve a high accuracy with fewer sampling points.

Generally, the used LG mode basis for expansion is strongly related to beam waist. To choose a suitable beam waist, one should have a clear knowledge of the radial feature of the LG beam. Figure 3(a) shows the radial distribution of the $LG_{l=6}^{p=50}$ mode with a beam waist w_0. Its amplitude oscillates along the radial direction. When the radius is small, the local oscillatory period increases slowly with the increase of the radius. The outer area, with an obviously larger period, offers limited spatial frequency for image decomposition. Thus, we define the region where the oscillatory period varies slowly as the effective area of the LG mode. In this work, we remove the outermost eight nodes and define the remaining inner part as the effective area. Figure 3(b) shows $B_{l=6}(r)$, i.e., the $l=6$ subspace of the image to be decomposed. One can calculate the spatial domain width $r_{l=6} = 0.0082$ m with 99% accuracy and the frequency domain width $f_{l=6} = 703.125 \, \text{m}^{-1}$ with 90% accuracy.
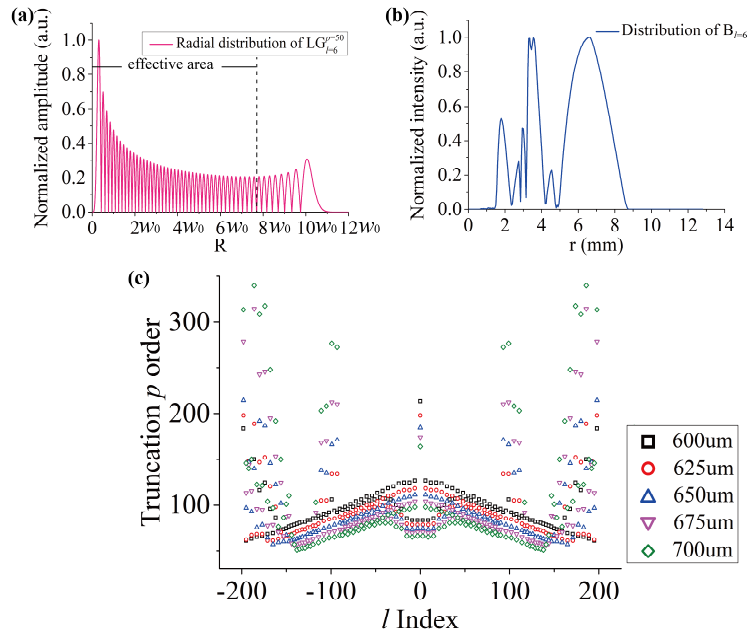
Fig. 3. Optimization of beam waist. (a) The radial distribution of LG mode ($l=6$, $p=50$) and its effective area. (b) The radial distribution of OAM subspace of $l=6$, (c) The truncation p order with different w_0.

To decompose the image, the effective area of the truncation LG mode must cover the radial distribution of the image and offer sufficiently high frequency. Therefore, the truncation order for

p is decided by the following criteria,

$$N_1^{l,p} w_0 > r_l \tag{9a}$$

$$2(N_1^{l,p} - N_2^{l,p})w_0 \le 1/f_l \tag{9b}$$

where $N_1^{l,p}$ and $N_2^{l,p}$ are the outermost and second outermost node of the effective area of LG mode. The value of w_0 should satisfy Eqs. (9a) and (9b) in all OAM subspaces.

Figure 3(c) shows the calculated truncation p order (i.e., the smallest p that satisfies Eq. (9a) and Eq. (9b)) with different w_0. A larger w_0 requires a lower truncation p order in general. However, the truncation p order in some OAM subspaces could be extremely high for large w_0. For example, when w_0 is 675um, the truncation p order in the $l = \pm 109$ subspace is 268, which indicates a sampling number of at least 269 to solve all the radial components by using least square fitting method. However, the maximal sampling number is 256 due to the limitation of the detector area in our experiment. Taking the above factors into consideration, we choose $650\,\mu m$ as the optimal w_0.
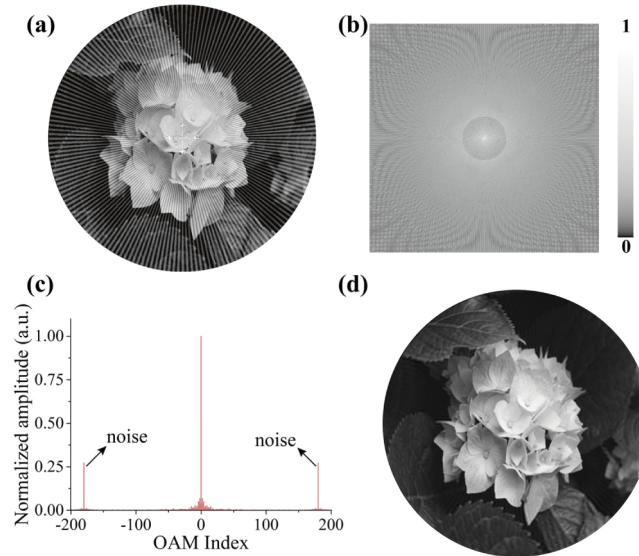
3. Results

By applying least square fitting, one can obtain the amplitude and phase LG spectrum of the image as shown in Figs. 4(a) and 4(b), respectively. Most of the condition numbers of matrices *LG* in Eq. (6) are lower than 10. The total LG mode number is 12647 and the reconstructed image is shown in Fig. 4(c). The structural similarity (SSIM) between the reconstructed image and the original image is 0.94, which demonstrates a good accuracy by using LG basis. In comparison, we also reconstruct the image by using Fourier basis with 12769 modes (Fig. 4(d)) and the corresponding SSIM is 0.79. Clearly, when decomposing an image with rotational symmetry, LG basis provides a higher image quality by using the same mode number.
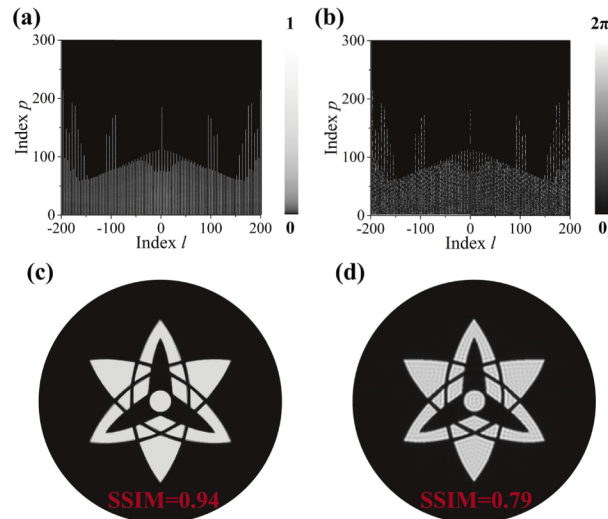
Fig. 4. Results of image decomposition in LG domain. (a) The amplitude of LG mode spectrum. (b) The phase of LG mode spectrum. (c) The reconstructed image by using 12647 LG modes in (a) and (b). (d) The reconstructed image by using 12769 Fourier components.

Linear CCD rotated scanning is a popular imaging method. However, high-frequency dark noise of the detector could introduce an azimuthal periodic noise, which has a severe influence on the recorded image (Fig. 5(a)). It is hard to recognize this kind of noise in Fourier domain as shown in Fig. 5(b). However, it is convenient to filter such noise in LG mode domain because

the major information for a natural image is carried by low-order LG modes. Figure 5(c) shows the l spectrum of the scanned image. The periodic noise exists near ±180-order. By using the l components ranging from −150 to 150, the recomposed image (Fig. 5(d)) clearly exhibits an improved quality.

Fig. 5. Results of image noise filtering. (a) Raw image with azimuthal noise recorded by linear CCD. (b) The corresponding Fourier spectrum. (c) The corresponding l spectrum. (d) The reconstructed image after LG domain filtering.

4. Conclusion

In conclusion, we have introduced an efficient approach to decompose an optical image based on LG modes. It is convenient to analyze the image of rotational symmetry by using the LG spectrum. The measured SSIM proves a high quality reconstruction. It should be noted that the reconstructive image by using LG mode is not perfect because an optical image is typically defined over a finite area. We have developed an effective method to significantly reduce the radial sampling number. The LG mode range for decomposing the image is related to the optimal beam waist. In addition, we experimentally demonstrate the azimuthal noise filtering in LG domain. Our results pave a way for utilizing LG-mode basis for optical image processing.

Disclosures. The authors declare no conflicts of interest.

References

1. T. Kuga, Y. Torii, N. Shiokawa, T. Hirano, Y. Shimizu, and H. Sasada, "Novel Optical Trap of Atoms with a Doughnut Beam," Phys. Rev. Lett. **78**(25), 4713–4716 (1997).
2. M. Dienerowitz, M. Mazilu, P. J. Reece, T. F. Krauss, and K. Dholakia, "Optical vortex trap for resonant confinement of metal nanoparticles," Opt. Express **16**(7), 4991 (2008).
3. N. Bozinovic, Y. Yue, Y. Ren, M. Tur, P. Kristensen, H. Huang, A. E. Willner, and S. Ramachandran, "Terabit-Scale Orbital Angular Momentum Mode Division Multiplexing in Fibers," Science **340**(6140), 1545–1548 (2013).

4. J. Wang, J. Yang, I. M. Fazal, N. Ahmed, Y. Yan, H. Huang, Y. Ren, Y. Yue, S. Dolinar, M. Tur, and A. E. Willner, "Terabit free-space data transmission employing orbital angular momentum multiplexing," Nat. Photonics **6**(7), 488–496 (2012).

5. R.-M. Monika, "Orbital angular momentum light in microscopy," Philos. Trans. R. Soc., A **375**, 20150437 (2017).

6. S. Xiao, L. Zhang, D. Wei, F. Liu, Y. Zhang, and M. Xiao, "Orbital angular momentum-enhanced measurement of rotation vibration using a Sagnac interferometer," Opt. Express **26**(2), 1997 (2018).

7. G. Verma and G. Yadav, "Compact picometer-scale interferometer using twisted light," Opt. Lett. **44**(14), 3594 (2019).

8. E. Nagali, L. Sansoni, F. Sciarrino, F. D. Martini, L. Marrucci, B. Piccirillo, E. Karimi, and E. Santamato, "Optimal quantum cloning of orbital angular momentum photon qubits through Hong–Ou–Mandel coalescence," Nat. Photonics **3**(12), 720–723 (2009).

9. A. Nicolas, L. Veissier, L. Giner, E. Giacobino, D. Maxein, and J. Laurat, "A quantum memory for orbital angular momentum photonic qubits," Nat. Photonics **8**(3), 234–238 (2014).

10. E. Yao, S. Franke-Arnold, J. Courtial, S. Barnett, and M. Padgett, "Fourier relationship between angular position and optical orbital angular momentum," Opt. Express **14**(20), 9071 (2006).

11. L. Torner, J. P. Torres, and S. Carrasco, "Digital spiral imaging," Opt. Express **13**(3), 873 (2005).

12. G. Molina-Terriza, L. Rebane, J. P. Torres, L. Torner, and J. Carrasco, "Probing canonical geometrical objects by digital spiral imaging," JEOS:RP **2**, 07014 (2007).

13. D. Petrov, N. Rahuel, G. Molina-Terriza, and L. Torner, "Characterization of dielectric spheres by spiral imaging," Opt. Lett. **37**(5), 869 (2012).

14. B. Jack, M. J. Padgett, and S. Franke-Arnold, "Angular diffraction," New J. Phys. **10**(10), 103013 (2008).

15. G. Xie, H. Song, Z. Zhao, G. Milione, Y. Ren, C. Liu, R. Zhang, C. Bao, L. Li, Z. Wang, K. Pang, D. Starodubov, B. Lynn, M. Tur, and A. E. Willner, "Using a complex optical orbital-angular-momentum spectrum to measure object parameters," Opt. Lett. **42**(21), 4482 (2017).

16. Z. Yang, O. S. Magaña-Loaiza, M. Mirhosseini, Y. Zhou, B. Gao, L. Gao, S. M. H. Rafsanjani, G. Long, and R. W. Boyd, "Digital spiral object identification using random light," Light: Sci. Appl. **6**(7), e17013 (2017).

17. W. Zhang, J. Gao, D. Zhang, Y. He, T. Xu, R. Fickler, and L. Chen, "Free-Space Remote Sensing of Rotation at the Photon-Counting Level," Phys. Rev. Appl. **10**(4), 044014 (2018).

18. F. Li, T. Xu, W. Zhang, X. Qiu, X. Lu, and L. Chen, "Optical images rotation and reflection with engineered orbital angular momentum spectrum," Appl. Phys. Lett. **113**(16), 161109 (2018).

19. L. Allen, M. W. Beijersbergen, R. J. C. Spreeuw, and J. P. Woerdman, "Orbital angular momentum of light and the transformation of Laguerre-Gaussian laser modes," Phys. Rev. A **45**(11), 8185–8189 (1992).

20. A. M. Yao and M. J. Padgett, "Orbital angular momentum: origins, behavior and applications," Adv. Opt. Photonics **3**(2), 161 (2011).

21. A. Mair, A. Vaziri, G. Weihs, and A. Zeilinger, "Entanglement of Orbital Angular Momentum States of Photons," Nature **412**(6844), 313–316 (2001).

22. J. Leach, M. J. Padgett, S. M. Barnett, S. Franke-Arnold, and J. Courtial, "Measuring the Orbital Angular Momentum of a Single Photon," Phys. Rev. Lett. **88**(25), 257901 (2002).

23. G. C. G. Berkhout, M. P. J. Lavery, J. Courtial, M. W. Beijersbergen, and M. J. Padgett, "Efficient Sorting of Orbital Angular Momentum States of Light," Phys. Rev. Lett. **105**(15), 153601 (2010).

24. G. Kulkarni, R. Sahu, O. S. Magaña-Loaiza, R. W. Royd, and A. K. Jha, "Single-shot measurement of the orbital-angular-momentum spectrum of light," Nat. Commun. **8**(1), 1054 (2017).

25. P. Zhao, S. Li, X. Feng, K. Cui, F. Liu, W. Zhang, and Y. Huang, "Measuring the complex orbital angular momentum spectrum of light with a mode-matching method," Opt. Lett. **42**(6), 1080 (2017).

26. A. Volyar, M. Bretsko, Y. Akimova, and Y. Egorov, "Measurement of the vortex spectrum in a vortex-beam array without cuts and gluing of the wavefront," Opt. Lett. **43**(22), 5635 (2018).

27. A. Volyar, M. Bretsko, Y. Akimova, and Y. Egorov, "Measurement of the vortex and orbital angular momentum spectra with a single cylindrical lens," Appl. Opt. **58**(21), 5748 (2019).

28. Y. Xiao, X. Tang, C. Wan, Y. Qin, H. Peng, C. Hu, and B. Qin, "Laguerre-Gaussian mode expansion for arbitrary optical fields using a subspace projection method," Opt. Lett. **44**(7), 1615 (2019).

29. A. D'Errico, R. D'Amelio, B. Piccirillo, F. Cardano, and L. Marrucci, "Measuring the complex orbital angular momentum spectrum and spatial mode decomposition of structured light beams," Optica **4**(11), 1350 (2017).